Communications Materials

https://doi.org/10.1038/s43246-026-01095-z

Article in Press

Shapiro steps in ballistic Josephson junction based on a single $Bi_2Te_{2.3}Se_{0.7}$ nanocrystal

Received: 26 January 2025

Accepted: 29 January 2026

Cite this article as: Stolyarov, V.S., Kozlov, S.N., Yakovlev, D.S. *et al.* Shapiro steps in ballistic Josephson junction based on a single $Bi_2Te_{2.3}Se_{0.7}$ nanocrystal. *Commun Mater* (2026). https://doi.org/10.1038/s43246-026-01095-z

V. S. Stolyarov, S. N. Kozlov, D. S. Yakovlev, O. V. Skryabina, D. S. Lvov, A. S. Vasenko, J. Zhou, M. Yu. Kupriyanov, A. A. Golubov, C. Feuillet-Palma, G. Ménard, N. Bergeal & D. Roditchev

Shapiro Steps in ballistic Josephson junction based on a single $Bi_2Te_{2.3}Se_{0.7}$ nanocrystal

V. S. Stolyarov[1,2,3,4*], S. N. Kozlov[1], D. S. Yakovlev[1], O. V. Skryabina[2], D. S. Lvov[2], A. S. Vasenko[4], J. Zhou[5], M. Yu. Kupriyanov[2,6], A. A. Golubov[2,4], C. Feuillet-Palma[1], G. Ménard[1], N. Bergeal[1], D. Roditchev[1]

[1]LPEM, ESPCI Paris, PSL Research University, CNRS, Sorbonne University, 75005 Paris, France.
[2]Advanced Mesoscience and Nanotechnology Centre, Moscow Institute of Physics and Technology, 141700 Dolgoprudny, Russia.
[3]Dukhov Research Institute of Automatics (VNIIA), 127055 Moscow, Russia.
[4]HSE University, Moscow 101000, Russia.
[5]Centre for Quantum Physics, Beijing Institute of Technology, Beijing 100081, China.
[6]Skobeltsyn Institute of Nuclear Physics, Lomonosov Moscow State University, 119991 Moscow, Russia.

*Corresponding author(s). E-mail(s): stolyarov.vs@phystech.edu;

Abstract

Josephson junctions based on topological insulators are expected to host Majorana-type bound states that promote a 4π-periodic current-phase relationship. One experimental consequence of this periodicity is the absence of odd Shapiro steps in the current-voltage characteristics under microwave radiation. Here, we experimentally study the frequency-dependent amplitude of Shapiro steps in a ballistic Josephson junction involving a 23 nm-thick single nanocrystal of topological insulator $Bi_2Te_{2.3}Se_{0.7}$ connected to two planar Nb-electrodes. We observe a progressive suppression of the first step while decreasing the frequency below 2 GHz. Using the two-channel thermal resistively shunted junction (tRSJ) model, we show that despite a ballistic regime, the overheating phenomena are enough to account for the observed effect. Our results highlight the complex physics of Josephson junctions and underscore that the missing first Shapiro step alone is not a definitive signature of topological superconductivity.

Keywords: Josephson junctions, Shapiro steps, ballistic transport, topological insulator, nanocrystals

1 Introduction

Proximity Josephson junctions (JJ) involve a non-superconducting material connected to two superconducting electrodes [1]. This geometry is widely used involving three-dimensional topological insulators (3D-TI) [2], 2D-TI [3] and, more recently, conventional III-V semiconducting heterostructures [4, 5]. Josephson junctions are attractive because the superconducting phase difference across the junction provides an additional degree of freedom for controlling the topological phase [3, 4, 5]. For this reason, the non-trivial 4π-periodicity of the current-phase relation (CPR) has recently attracted considerable experimental attention [6, 7, 8, 9, 10]. The phenomenon arises from Andreev bound states (ABS) crossing the zero (Fermi) energy when the phase φ between superconducting leads of the JJ is π. In the topological case, such an intersection is protected by the conservation of fermionic parity [11, 3, 12]. After crossing the ABS levels at $\varphi = \pi$, the system is no longer in the ground state for $\pi < \varphi < 3\pi$, and tends to relax. As a consequence, the observation of the 4π-periodic term in the Josephson current requires the CPR measurements at frequencies exceeding the rate of equilibration processes [12, 13, 14]. The presence of such an oscillating current leads to several predicted effects associated with topological superconductivity [15, 16, 17, 18, 9].

When a Josephson junction is exposed to microwave radiation of a frequency f_{RF}, the resulting periodic variation of the bias current through the junction can modulate the phase shift between the superconducting contacts. When this modulation is phase-locked to the fundamental self-frequency f_J of the Josephson junction, $n \cdot f_{RF} = f_J$ (n being an integer), constant voltage (Shapiro) steps [21] appear in the DC $V(I)$ characteristics at DC-voltages $V = \langle V(t) \rangle = n \cdot h\, f_{RF}/2e$. The appearance of Shapiro steps is a direct consequence of the Josephson relation linking the time-derivative of the phase to the voltage drop, $\frac{\partial \varphi}{\partial t} = 2eV/\hbar$. In trivial JJ, the CPR is 2π-periodic [21, 22] leading to a series of Shapiro steps $n = 1, 2, 3, ...$ However, when topological superconductivity is present, the CPR is 4π-periodic, which ideally results in the absence of odd Shapiro steps [7, 23]. The analysis of Shapiro steps involves characteristic frequencies $f_{4\pi}$ and $f_{2\pi}$, as initially introduced by Dominguez *et al.* [24]

The missing first Shapiro steps (MFS) effect has indeed been observed in systems involving 3D-TI HgTe quantum wells (QW) [15], 2D-TI HgTe QW [16], spin-orbit coupled semiconductor nanowires [18, 9, 25, 26, 27], and Dirac semimetals [28, 29]. In particular, high-intensity drives exhibited residual supercurrent, further confirming the 4π-periodic nature of the AC-Josephson effect [30]. Later experiments on HgTe/CdTe-based junctions demonstrated the absence of the first nine odd steps [16] along with observing the fractional Josephson radiation frequency. These experiments were consistently interpreted as strong evidence of a topological superconducting (TS) state. Indeed, the absence of Shapiro steps in trivial systems has not been detected

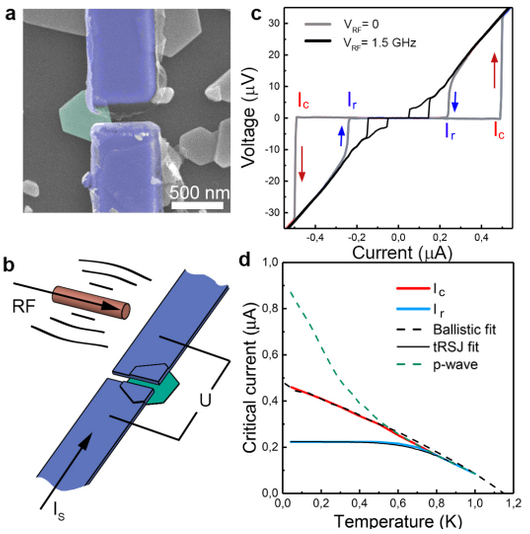

Fig. 1 Experimental observation of supercurrent in Josephson junction based on a single nano-crystal of $Bi_2Te_{2.3}Se_{0.7}$. **a** – Scanning electron microscopy image of the Nb/$Bi_2Te_{2.3}Se_{0.7}$/Nb Josephson junction. Conventional superconducting Nb-leads are false-colored in blue; the flake of $Bi_2Te_{2.3}Se_{0.7}$ with unconventional induced superconductivity is false-colored in light-green. **b** – Schematic view of the device and the external electrical circuit. DC-bias current I is applied and the voltage drop V is measured across the junction. **c** – Hysteretic $V(I)$ characteristic of the junction measured at $T = 20$ mK. Without RF-excitation, the junction showed a critical current I_c=0.46 μA (red arrows) and a retrapping current I_r=0.22 μA (blue arrows). Upon RF-excitation, $V(I)$ curves demonstrate several Shapiro steps (black line, measured at f_{RF}=1.5 GHz, V_{RF}=20 μV). **d** – Temperature dependence of the critical current I_c (red line) and the retrapping current I_r (blue line). The ballistic fit of $I_c(T)$ (black dashed line) was performed using the Eilenberger equations with the same parameters as in [19]. The $I_R(T)$ dependence was fitted by the tRSJ model (black solid line, see details in the main text). The green dashed line reproduces the maximum critical current observed on the same JJ in our earlier work [20].

so far or, when observed, the effect was weak [31]. Though, it has been noted that Landau-Zener transitions between ABS could also produce similar features [32, 24, 33].

The demonstration of the suppression of odd Shapiro steps along with the fractional frequency of Josephson radiation are considered to be the possible routes to prove the existence of the Majorana zero modes (MZM) [24, 13, 34, 15, 35]. Compared to diffuse JJ, ballistic proximity junctions exhibit ABS energies with a 4π-periodic dependence [36] $\pm\Delta\cos(\varphi/2)$, where Δ is the proximity-induced energy gap. However, despite this similarity with MZMs, the CPR of such junctions remains 2π-periodic. The MFS effect could also originate from trivial ballistic transport, to differentiate among the different possible interpretations. The ubiquity of the MFS effect includes observations in amorphous superconducting nanowires and nanobridges [37]. Note that the first or even several low-index steps could also be masked by JJ switching at the critical I_c or retrapping currents I_r.

In previous work [20], we identified a significant component of TS in ballistic JJ involving a single nanocrystal of $Bi_2Te_{2.3}Se_{0.7}$ [19]. This was reflected in the form

of resonant oscillations of the critical current under a magnetic field and associated with the formation of peculiar Andreev levels. This discovery motivated us to provide experimental measurements of current-voltage characteristics under microwave radiation on the same ballistic JJ. The main result of these experiments we report here is the demonstration of missing $n = 1$ Shapiro steps. We present numerical calculations within the thermal resistively shunted junction (tRSJ) model [30] which show that even in our case of high-quality ballistic JJ, the missing first Shapiro steps may originate from overheating effects and not necessarily be related to TS-induced 4π-component of the supercurrent. We also discuss the possibility of the first Shapiro step suppression in the vicinity of the retrapping current via the mechanism recently suggested by S. Ustavschikov et al. [38].

2 Results and Discussion

Experimental setup and cryogenic measurements.

The synthesis of $Bi_2Te_{2.3}Se_{0.7}$ nanocrystals and the fabrication of nanocrystal-based JJ are presented in detail in our previous works [39, 19]. The top view SEM image of the studied JJ is presented in Fig.1a. The measured thickness of the nanocrystal (false-colored in green) is $t = 23$ nm, the length of the TI region is $L = 150$ nm, and the Nb electrode widths are $w = 500$ nm. Fig.1b provides a schematic view of the Josephson junction connected to the external electrical circuit, including an RF-antenna. The room temperature resistance of the junction is $R_n \approx 1.2$ kΩ, which includes the part of the niobium nanowire and interface resistance [19]. Upon cooling, the resistance shows a conventional metallic $R(T)$ behavior. An abrupt drop in $R(T)$ is detected at $T = 8$ K; it is attributed to the superconducting transition of the Nb electrodes of the junction. Further cooling down from 5 to 1 K shows a smooth decrease in $R(T)$ characteristic of the superconducting proximity effect induced in the TI flake by closely spaced Nb electrodes [19]. Below about 1.5 K, the junction is fully superconducting and the effective normal-state resistance of the junction channel in the superconducting regime R_J starts to be several tens Ω. [19, 20]. Hysteretic current-voltage characteristics $I(V)$, measured at 20 mK with a high-level filtering system [40], are shown in Fig. 1c. The IV curves were measured by sweeping the bias current in the sequence $0 \to +I_{max} \to 0 \to -I_{max} \to 0$ while continuously recording the voltage. They demonstrate the difference between the critical current (I_c) measured in the forward direction (increasing current) and the retrapping current (I_r, measured when decreasing current). The red and blue curves illustrate the hysteretic asymmetry of the $V(I)$ characteristics. The asymmetry originates from Joule overheating [41], which is considered to be a source of quasi-particle poisoning [42]. The black curve illustrates the $V(I)$ DC-characteristic acquired in the presence of an RF-signal. Fig. 1d displays the temperature dependence of both the critical and the retrapping currents. Hysteresis appears at temperatures below 0.7 K. Additionally, the absence of a low-temperature saturation in the $I_c(T)$ curve suggests ballistic transport, which is further supported by fits generated using the ballistic limit of Eilenberger equations [36] (black dashed line in Fig. 1d). From the measured V(I) curve, we can estimate the effective normal-state resistance of the junction channel in the

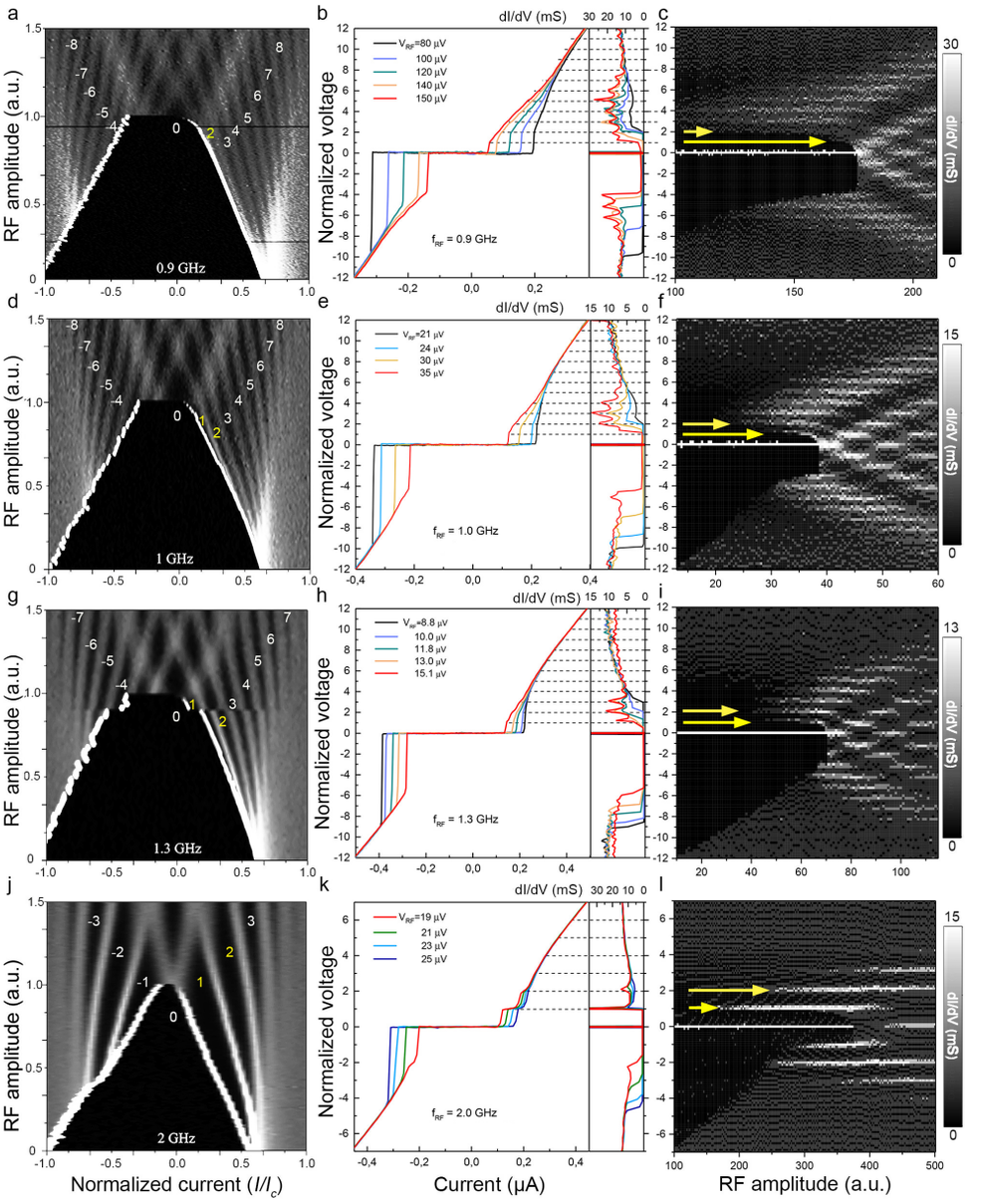

Fig. 2 Shapiro maps recorded at T =20 mK for different RF-drive frequencies and amplitudes. a – grey-scale differential resistance map $dV/dI(I_{DC}/I_c, V_{RF}/V_{RF}(I_c = 0))$ recorded at $f_{RF} = 0.9$ GHz. **b** – a series of $V(I)$ curves and their $dI/dV(V)$ plots taken at selected amplitudes of RF-excitation. **c** – grey-scale differential conductance map $dI/dV(V, V_{RF})$; yellow arrows mark the first and the second Shapiro steps. The voltage scale (vertical) is presented in numbers of Shapiro steps, $n = 2eV/hf_{RF}$. **d,e,f** – the same as in **a**, **b** and **c** but for f_{RF}=1 GHz, **g,h,i** – for f_{RF}=1.3 GHz, and **j,k,l** – for f_{RF}=2 GHz, respectively.

superconducting regime $R_J \approx 80\Omega$. To achieve that value in the ballistic regime, we need the following number of channels $N = \frac{h}{2e^2 R_J} \approx 160$. That number is correlated to the number of topological surface channels $N_{2D} \approx \frac{2W_{crys}}{\lambda_F}$, where W_{crys} is a width of the crystal and λ_F is the Fermi length of the topological channel $\lambda_F = \frac{2\pi}{k_F} \approx 6nm$, where k_F is the Fermi wavevector. Using this estimation, the number of topological surface channels is $N_{2D} \approx 147$. That is closed to the value that is needed to obtain the experimental normal resistance R_J. Discrepancies can be due to the volumetric shunting effect, which is consistent with our model.

Microwave experiment.

Fig. 2 demonstrates the influence of microwave radiation on the electron transport properties of the JJ shown in Fig.1a. Measurements of the critical current as a function of frequency at constant RF power (Supplementary Figure 1) revealed optimal coupling conditions at RF frequencies of 0.9, 1, 1.3, and 2 GHz. These frequencies were selected for detailed Shapiro step analysis as they provided maximum suppression of I_c, indicating efficient RF power delivery to the junction. Fig. 2a shows the differential resistance $dV/dI(I_{DC}, V_{RF})$ map as a function of normalized RF voltage and normalized current across the JJ for f_{RF} =0.9 GHz. There, the RF amplitude is normalized to $V_{RF}(I_c = 0)$, and the current is normalized to the critical current of the JJ in the absence of RF radiation. On this map, the dark-grey areas correspond to low differential resistance at the Shapiro steps, light-grey lines - to the differential resistance maxima between adjacent Shapiro steps, black background (the area under the number 0) - to zero voltage across the JJ when it is in the stationary Josephson regime.

The improved visibility of Shapiro steps with increasing frequency is a well-known phenomenon. For instance, this effect is clearly demonstrated in terms of the characterisic frequency $\Omega = \Phi_0 v_{ac}/2\pi R_J I_c$ in Refs. [43, 44, 45, 46]. Consequently, at lower frequencies, distinguishing between steps becomes more challenging, especially at low RF amplitudes. This difficulty could also obscure the observation of the first Shapiro step.

The concept of odd-even effect in Shapiro steps unrelated to a 4π-periodic contribution to the current-phase relationship has been discussed in [47], where only even or odd steps appear at specific RF amplitudes, an effect known as the odd-even effect. To draw conclusions about the current-phase relationship and its variations under different conditions, a complete Shapiro map must be considered. As demonstrated in Refs. [45] and [46], a higher harmonic contribution (e.g., a skewed current-phase relationship) only becomes evident at sufficiently high reduced frequencies. In those studies, Ω was increased by reducing I_c through an externally applied magnetic field to meet this criterion.

The asymmetry of the right and left parts of the graph relative to $I/I_c = 0$ is due to the presence of overheating hysteresis in the $I(V)$ curves (see Fig.1c), which determinates I_c and I_R. At currents exceeding the critical and retrapping currents ($|I| > I_c, I_R$), a voltage drop appears (non-stationary Josephson regime of JJ) which, in the presence of external microwave radiation, leads to characteristic Shapiro steps. The steps are visible in alternating light and dark stripes numbered from n=-8 to n=+8 (negative numbers correspond to negative values of I/I_c). For clarity, Fig. 2b

shows the $V(I)$-curves along with their derivatives taken at selected amplitudes of RF radiation of a f_{RF} =0.9 GHz, V_{RF} =80, 100, 120, 140, and 150 μV, shown in black, blue, green, yellow and red lines, respectively. Here, the normalized voltage axis is graduated in numbers of the Shapiro steps. Figure 2c is a layout of the Shapiro steps for $dI/dV(V)$ as a function of V_{RF}. Figure 2c clearly shows that the counting of the observed Shapiro steps begins at $n = 4$, in the negative voltage region, and at $n = 2$, in the positive region. Thus, it is clear that the first Shapiro steps are missing. Similar studies were also carried out at RF frequencies 1 GHz (Fig.2d,e, f), 1.3 GHz (Fig.2g,h,i) and 2 GHz (Fig.2j,k,l), respectively. The yellow arrows in (Fig.2c,f,i,l) show the evolution of the appearance of the first and second Shapiro steps. In this case, the first Shapiro step only appears in the retrapping branch of the $V(I)$ curve. The first Shapiro step is consistently present at frequency f_{RF}=1.3 GHz and higher. Additional measurements at 0.5 GHz (Supplementary Figure 2) further confirm the suppression of the first Shapiro step at frequencies below 1 GHz, though with reduced step visibility due to smaller voltage spacing between steps.

Overheating and retrapping current.

A common characteristic, observed at all frequencies, is that all steps are visible when the RF-excitation is sufficiently strong (see the upper parts of the plots in Figs.3a,b). This occurs because, for sufficiently large V_{RF}, both the critical current and the retrapping current drop to zero, while the superconducting order parameter remains non-zero. Under these conditions, the DC voltage gradually increases with the DC bias current. As a result, all low-order steps are visible, and there are no missing steps at sufficiently large amplitude of the RF-drive, V_{RF}. In Figs3a,b, all steps are marked with yellow lines, while blue dashed lines indicate the switching (I_c) and retrapping (I_R) currents. The main difference between the high-frequency data (2 GHz) (Fig.3a) and the low-frequency data (1 GHz) (Fig.3b) is that, in the former, the slope of the yellow lines is steeper than the slope of the retrapping current blue dashed lines, whereas in the latter the slopes are similar. Additionally, the spacing between the yellow lines (the steps) is naturally smaller when the RF signal has a lower frequency since the voltage difference between the steps is $hf_{RF}/2e$.

On the other hand, at high RF frequency, there is a significant space between the retrapping (dashed blue) line and the second Shapiro step (yellow) line where at least a part of the first Shapiro plateau should be observable experimentally, even at low RF-drive (Figs.3a,b).

Modelling and discussion.

Recently, Le Calves et al. [30], suggested a method to distinguish between topological and trivial effects by carefully considering the role of quasiparticle poisoning due to Joule heating. A high population of quasiparticles causes stochastic changes in Majorana Zero Energy Modes occupation, altering the parity and averaging the 4π-periodic contribution to the junction CPR to zero. The partial even-odd effect in topological Josephson junctions, i.e. the absence of the first Shapiro steps at low RF-power while higher order steps are present, is therefore controlled by the interplay between the characteristic switching parity lifetime caused by the overheating effect and the Josephson phase relaxation time. For long switching times (low current bias), quasiparticle poisoning is limited, and the first Shapiro steps are not visible, whereas

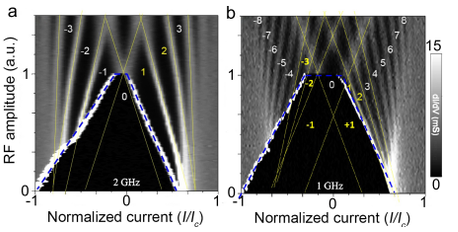

Fig. 3 Retrapping current overlapping Shapiro steps. a and **b** – Differential resistance versus normalized bias current and RF drive amplitude. The retrapping currents and the switching currents (blue dashed lines) form the main borders of a trapezoidal zero-resistance region. Thin yellow lines delimit different RF-induced Shapiro steps. (**a**) – at $f_{RF} = 2\,\mathrm{GHz}$, the first Shapiro step ($V_{n=1} = hf_{RF}/2e$) is clearly observed. (**b**) – at $f_{RF} = 1\,\mathrm{GHz}$, the first step shows up only at high RF-amplitude. At low RF-drive, the junction transits from the superconducting state to the second Shapiro step ($V_{n=2} = hf_{RF}/e$) directly, without entering the first step.

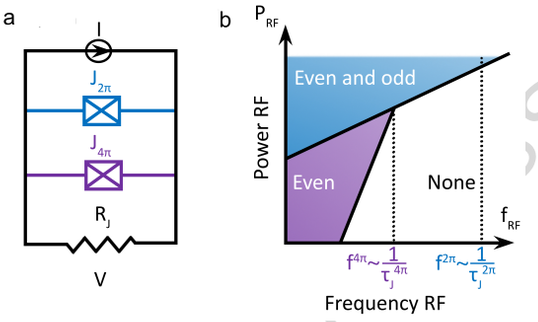

Fig. 4 Two-channel tRSJ model. a – two parallel Josephson junctions, the trivial ($J_{2\pi}$) and the topological ($J_{4\pi}$), are put in parallel with the shunt resistance R_J. They are characterized by two different critical currents and current–phase periodicities, that is, $I_s = I_c^{2\pi}\sin(\varphi)$, and $I_s = I_c^{4\pi}\sin\left(\frac{\varphi}{2}\right)$, respectively. **b** – phase diagram showing the range of existence of even and odd Shapiro steps as a function of radio-frequency (RF) drive frequency f_{RF} and RF power P_{RF}. The boundaries indicate the cutoff frequencies $f^{2\pi}$ and $f^{4\pi}$, above which the 2π- and 4π-periodic channels, respectively, can no longer follow the drive and their contributions to the Shapiro steps are strongly suppressed.

for short switching times (high current bias), the 4π-periodic Josephson component is suppressed, and odd steps are visible. The ballistic electron theory of SNS junctions accurately describes the temperature evolution $I_c(T)$. In the dissipative regime of the current-voltage characteristic, Joule heating is significant, especially on the return branch, where heating occurs down to the retrapping. Thus, in the return branch, quasiparticle poisoning is expected to occur down to the retrapping current and, consequently, the first step should be observable. In our experiments, however, the first step is still missing in the retrapping current branch despite intense Joule heating, which is responsible for a pronounced hysteresis of the $V(I)$ curves, and consequently, for a quasiparticle poisoning. A rapid conclusion would be that the 4π-component of the CPR is not completely suppressed. Though, as we discuss below, an alternative and more traditional explanation of the observed result is possible, not necessarily involving TS.

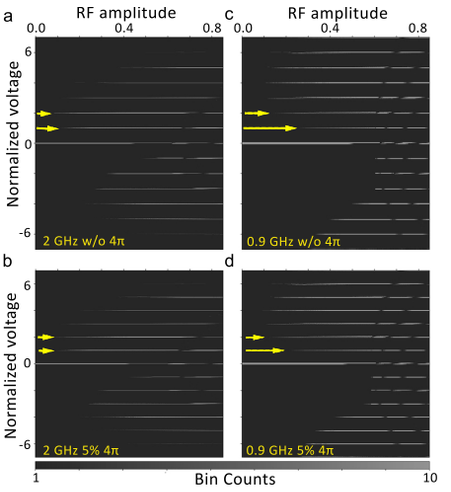

Fig. 5 Simulated Shapiro maps. Color-coded histograms of Shapiro steps maps as a function of the RF-current for RF-frequencies (**a,b**) – 2 GHz, without and with 5% 4π-component, and (**c,d**) – 0.9 GHz, without and with 5% 4π-component. Shapiro steps $n = 1$ and $n = 2$ are marked by yelow arrows.

The observed hysteresis and the detailed structure of the Shapiro steps cannot be fully described within the framework of the standard RSJ model which does not consider overheating effects, and thus is inapplicable in high voltage and current range causing a significant Joule heating. Therefore, we model our system using the two-channel tRSJ approach proposed in [30, 48]. With respect to a standard RSJ approach, this model includes two more ingredients: an additional 4π-periodic coherent superconducting channel originating from Majorana bound states and a self-consistent heat equation that balances Joule heating and phonon cooling. In Fig.4a, the scheme of the two-channel tRSJ model is shown. The JJ is represented there by trivial ($\mathrm{J}_{2\pi}$) and topological ($\mathrm{J}_{4\pi}$) branches put in parallel and shunted by the resistance R. The topological branch is characterized by 4π-CPR. The total superconducting current is $I_s(\varphi) = I_c^{2\pi}\sin(\varphi) + I_c^{4\pi}\sin(\varphi/2)$, and the equation for the phase dynamics can be written as

$$\frac{\hbar d\varphi}{2eR_J dt} = I_{DC} + I_{RF}\sin\left(2\pi f_{RF} t\right) - \left(I_c^{2\pi}\sin(\varphi) + I_c^{4\pi}\sin(\varphi/2)\right), \tag{1}$$

where I_{DC} is the DC bias current, I_{RF} is the amplitude of the RF excitation, $I_c^{2\pi}$ $\left(I_c^{4\pi}\right)$ is the critical current of 2π- $(4\pi-)$ component, R_J is the normal state resistance of the junction.

To take into account the hysteretic behavior of $V(I)$ characteristics due to Joule overheating, we write the heat balance equation [30]:

$$\langle P(t)\rangle = \Sigma U\left(T_e^5 - T_{ph}^5\right), \tag{2}$$

where Σ is the electron-phonon coupling constant, U is the effective volume, T_e and T_{ph} are electron and phonon temperatures of the system, respectively. The self-consistent calculation scheme proceeds as follows: For given values of I_{DC} and I_{RF}, we start by assuming a temperature T (at the first iteration, $T = T_{ph}$, equal to the cryostat bath temperature). This provides a critical current $I_c(T) = I_c^{2\pi}(T) + I_c^{4\pi}(T)$. Next, we solve Eq.1, estimate the Joule power $P = \langle I(t)V(t)\rangle$, which determines the temperature of the electron subsystem $T_e = \sqrt[5]{{T_{ph}}^5 + \frac{P}{\Sigma U}}$, and subsequently, a new critical current $I_c(T_e)$. This process is repeated i-times until the difference between the new estimated temperature T^{i+1} and the previous temperature T^i is considered satisfactorily small. The temperature dependence of the critical current $I_c(T)$ is derived from the ballistic fit, and the parameters Σ and U are extracted from the retrapping current fit I_R (see Fig.1). For clarity we have also included electron temperature plot as Supplementary Figure 3 for the frequency equals 2 GHz with a 5% 4π-contribution.

As shown by Le Calvez *et al.* [30], this system exhibits two characteristic frequencies, $f^{2\pi} = 2eR_J I_c^{2\pi}/\hbar$ and $f^{4\pi} = eR_J I_c^{4\pi}/\hbar$, which correspond to the phase relaxation times $\tau_{2\pi} = 1/f^{2\pi}$ and $\tau_{4\pi} = 1/f^{4\pi}$ for the 2π- and 4π-periodic channels, respectively. These frequencies set the cutoff above which the contribution of each channel to the Shapiro steps is strongly suppressed, and they define the two-dimensional phase diagram shown in Fig. 4b. Color plots in Fig. 5a,b present the results of numerical calculations performed using the model for a frequency of 0.9 GHz. The results demonstrate that the second step appears first at low RF-power, while the first step emerges at higher power. As shown in Figure 5c,d, the model can reproduce our experimental data at a frequency of 2 GHz with a zero-amplitude of 4π-periodic component. It also captures well the zero-resistance region at low DC and RF bias, including the linear boundary shape. Including a 5% 4π-periodic contribution leads to improved alignment between the simulation and experimental RF-power dependence of the $n = 1$ and $n = 2$ steps, particularly at intermediate drive amplitudes. However, it also introduces a partial suppression of the $n = 3$ step at 0.9 GHz, which is not as clearly visible in the experimental data. This discrepancy suggests that if a 4π contribution is present, it is likely small and its effects remain intertwined with circuit-related and thermal dynamics.

The observed suppression of n =1 Shapiro step could also be caused by its proximity to the retrapping current, where the JJ resistance rapidly changes. Recently, S. Ustavschikov et al. [38] theoretically demonstrated that in non-hysteretic JJs, a large differential resistance near the transition to the superconducting state prevents the phase locking to the RF-excitation frequency. This results in vanishing width of low-lying Shapiro steps. The authors found that if the differential resistance $R_{diff} = dV/dI$ at voltage $V_n = nf_{RF}h/2e$ of the considered step n significantly exceeds $R_{diff}(V_n)$ predicted by the overdamped Resistively and Capacitively Shunted Junction (RCSJ) model, the width of n-th Shapiro step reduces significantly or disappears. The same effect could be expected in our ballistic JJ near the retrapping current where the differential resistance becomes extremely high (compare $R_{diff}(V)$ plots and n =1 step amplitudes in Figs.2b,e,h,k).

We now confront the obtained results with the conclusions of our recent paper [20] reporting the discovery of fine oscillations of the critical current in the magnetic field

$I_c(H)$. The latter were attributed to the presence in the JJ of a significant amount of p-wave superconductivity induced, in parallel to the trivial one, by the proximity effect. These conclusions are in apparent contradiction with the results of the present study, which do not require any significant contribution of TS to be understood. Note that the temperature evolution of the retrapping current $I_R(T)$ (blue line) presented in Fig. 1d is exactly the same as the one determined for this JJ in previous works [19, 20]. Also, the minima of the oscillations $I_c(H)$ measured in [20] follow exactly the critical current $I_c(T)$ found in the present work (red line in Fig. 1d). Though in [20], the maxima of the oscillations appeared at a significantly higher critical current $I_{osc}(T)$, shown as a green dashed line in Fig. 1d. In the present work, this higher critical current branch $I_{osc}(T)$ with its peculiar upturn at low temperatures specific to p-wave TS [12] was not observed. Rather, the measured critical current $I_c(T)$ is lower and tends to saturate at low temperatures.

In [20], the critical current oscillations $I_c(H)$ due to p-wave component ranged between $I_{osc}(T)$ and $I_c(T)$. This TS channel exists in parallel to the trivial one; the latter is characterized by the critical current $I_c(T)$ - identical to what we found here (red line in Fig. 1d). With this idea in mind, we must admit that in the present work the TS component was (almost) absent or not probed. We can advance at least two reasons for this: 1) – sample degradation upon thermal cycling: the materials used in JJ have different thermal expansion coefficients; rigid Nb-electrodes overlapping a fragile lamellar TI-nanocrystal could create a strong mechanical tension leading to an important strain or even a partial exfoliation of the TI . While very much plausible [49], this hypothesis is difficult to reconcile with identical $I_c(T)$ and $I_R(T)$ characteristics observed in [19, 20] and in the present work; 2) — RF-environment: the presence of a RF-antenna necessary for Shapiro experiment could lead to an uncontrolled excitation of the fragile p-wave (surface) component of the superconducting order. Note that in the DC-experiment [20], the AC components were strongly rejected by a careful multi-stage filtering of all DC lines and by a specially shielded configuration of the sample holder, which was not appropriate for the RF-experiment.

2.1 Conclusion.

In conclusion, ballistic planar Josephson junctions involving a single nanocrystal of topological insulator $Bi_2Te_{2.3}Se_{0.7}$ demonstrate a progressive suppression of the first Shapiro step at frequencies below 2 GHz, with a strong reduction below 1.3 GHz. We show that this behavior is satisfactorily accounted for by the thermal resistively shunted junction model, taking into account the overheating and heat dissipation effects. Our analysis reveals that 4π-periodic CPR channel contribution is small and its influence remains intertwined with circuit-related and thermal dynamics. Our results demonstrate that the absence of the first Shapiro step does not provide the definitive evidence of topological superconductivity, as it can be robustly accounted for by conventional thermal effects.

2.2 Data availability.

A Data availability statement was added to the manuscript in the dedicated section. It specifies that all relevant data are available from the corresponding author upon reasonable request, including contact details (stolyarov.vs@phystech.edu).

3 Acknowledgements

Sample preparation was supported by the Ministry of Science and Higher Education of the Russian Federation (Grant No. 075-15-2025-010). The research was supported by the Russian Science Foundation, project No. 25-42-00058 https://rscf.ru/en/project/25-42-00058/ (cryogenic Shapiro steps measurements and theoretical analysis), NB and DR acknowledg ANR project CrysTop.

4 Author contributions

V.S.S. proposed the experimental concept. V.S.S. and D.R. jointly conceived the project and supervised the experimental work. D.S.Ya. and O.V.S. fabricated the samples. Low-temperature measurements were performed by V.S.S., C.F.-P., and G.M. Data analysis was conducted by V.S.S., S.N.K., D.S.Ya., D.S.L., A.S.V., J.Z., and N.B. Numerical modeling was carried out by S.N.K., M.Yu.K., and A.A.G. The manuscript was written by D.R., V.S.S., S.N.K., and D.S.Ya., with substantial contributions from all co-authors.

5 Additional information

5.1 Supplementary Information

accompanies this paper at https://doi.org/.....

5.2 Competing interests:

The authors declare no competing interests.

5.3 Reprints and permission

Information is available online at http://npg.nature.com/ reprintsandpermissions/

5.4 Publisher's note:

Springer Nature remains neutral with regard to jurisdictional claims in published maps and institutional affiliations.

References

[1] Sergey Bakurskiy et al. "Thouless energy in Josephson SN-N-NS bridges". In: *Mesoscience and Nanotechnology* 1.1 (July 2024), p. 01003. DOI: 10.64214/jmsn.01.01003.

[2] Liang Fu and Charles L Kane. "Superconducting proximity effect and Majorana fermions at the surface of a topological insulator". In: *Physical review letters* 100.9 (2008), p. 096407.
[3] Liang Fu and Charles L Kane. "Josephson current and noise at a superconductor/quantum-spin-Hall-insulator/superconductor junction". In: *Physical Review B* 79.16 (2009), p. 161408.
[4] Michael Hell, Martin Leijnse, and Karsten Flensberg. "Two-dimensional platform for networks of Majorana bound states". In: *Physical review letters* 118.10 (2017), p. 107701.
[5] Falko Pientka et al. "Topological superconductivity in a planar Josephson junction". In: *Physical Review X* 7.2 (2017), p. 021032.
[6] M Snelder et al. "Andreev bound states and current-phase relations in three-dimensional topological insulators". In: *Physical Review B—Condensed Matter and Materials Physics* 87.10 (2013), p. 104507.
[7] F Domınguez et al. "Josephson junction dynamics in the presence of 2 π-and 4 π-periodic supercurrents". In: *Physical Review B* 95.19 (2017), p. 195430.
[8] G Tkachov. "Chiral current-phase relation of topological Josephson junctions: A signature of the 4 π-periodic Josephson effect". In: *Physical Review B* 100.3 (2019), p. 035403.
[9] Dominique Laroche et al. "Observation of the 4π-periodic Josephson effect in indium arsenide nanowires". In: *Nature communications* 10.1 (2019), p. 245.
[10] Ian Babich et al. "Limitations of the current–phase relation measurements by an asymmetric dc-SQUID". In: *Nano Letters* 23.14 (2023), pp. 6713–6719.
[11] A Yu Kitaev. "Unpaired Majorana fermions in quantum wires". In: *Physics-uspekhi* 44.10S (2001), p. 131.
[12] H-J Kwon, K Sengupta, and Victor M Yakovenko. "Fractional ac Josephson effect in p-and d-wave superconductors". In: *The European Physical Journal B-Condensed Matter and Complex Systems* 37.3 (2004), pp. 349–361.
[13] Driss M Badiane et al. "Ac Josephson effect in topological Josephson junctions". In: *Comptes Rendus Physique* 14.9-10 (2013), pp. 840–856.
[14] DI Pikulin and Yuli V Nazarov. "Phenomenology and dynamics of a Majorana Josephson junction". In: *Physical Review B* 86.14 (2012), p. 140504.
[15] Jonas Wiedenmann et al. "4π-periodic Josephson supercurrent in HgTe-based topological Josephson junctions". In: *Nature communications* 7.1 (2016), p. 10303.
[16] Erwann Bocquillon et al. "Gapless Andreev bound states in the quantum spin Hall insulator HgTe". In: *Nature Nanotechnology* 12.2 (2017), pp. 137–143.
[17] Russell S Deacon et al. "Josephson radiation from gapless Andreev bound states in HgTe-based topological junctions". In: *Physical Review X* 7.2 (2017), p. 021011.
[18] Leonid P Rokhinson, Xinyu Liu, and Jacek K Furdyna. "The fractional ac Josephson effect in a semiconductor–superconductor nanowire as a signature of Majorana particles". In: *Nature Physics* 8.11 (2012), pp. 795–799.

[19] Vasily S Stolyarov et al. “Josephson current mediated by ballistic topological states in $Bi_2Te_{2.3}Se_{0.7}$ single nanocrystals”. In: *Communications Materials* 1.1 (2020), p. 38.

[20] Vasily S Stolyarov et al. “Resonant Oscillations of Josephson Current in Nb-$Bi_2Te_{2.3}Se_{0.7}$-Nb Junctions”. In: *Advanced Quantum Technologies* 5.3 (2022), p. 2100124.

[21] Sidney Shapiro. “Josephson currents in superconducting tunneling: The effect of microwaves and other observations”. In: *Physical Review Letters* 11.2 (1963), p. 80.

[22] Richard L Kautz. “Noise, chaos, and the Josephson voltage standard”. In: *Reports on Progress in Physics* 59.8 (1996), p. 935.

[23] Jordi Picó-Cortés, Fernando Domınguez, and Gloria Platero. “Signatures of a 4 π-periodic supercurrent in the voltage response of capacitively shunted topological Josephson junctions”. In: *Physical Review B* 96.12 (2017), p. 125438.

[24] Fernando Domınguez, Fabian Hassler, and Gloria Platero. “Dynamical detection of Majorana fermions in current-biased nanowires”. In: *Physical Review B* 86.14 (2012), p. 140503.

[25] Vincent Mourik et al. “Signatures of Majorana fermions in hybrid superconductor-semiconductor nanowire devices”. In: *Science* 336.6084 (2012), pp. 1003–1007.

[26] Anindya Das et al. “Zero-bias peaks and splitting in an Al–InAs nanowire topological superconductor as a signature of Majorana fermions”. In: *Nature Physics* 8.12 (2012), pp. 887–895.

[27] Andrea Iorio et al. “Half-integer Shapiro steps in highly transmissive InSb nanoflag Josephson junctions”. In: *Physical Review Research* 5.3 (2023), p. 033015.

[28] Chuan Li et al. “4π-periodic Andreev bound states in a Dirac semimetal”. In: *Nature materials* 17.10 (2018), pp. 875–880.

[29] Daniel Rosenbach et al. “Reappearance of first Shapiro step in narrow topological Josephson junctions”. In: *Science advances* 7.26 (2021), eabf1854.

[30] Kévin Le Calvez et al. “Joule overheating poisons the fractional ac Josephson effect in topological Josephson junctions”. In: *Communications Physics* 2.1 (2019), p. 4.

[31] Vlad S Pribiag et al. “Edge-mode superconductivity in a two-dimensional topological insulator”. In: *Nature nanotechnology* 10.7 (2015), pp. 593–597.

[32] P-M Billangeon et al. “Ac Josephson effect and resonant Cooper pair tunneling emission of a single Cooper pair transistor”. In: *Physical review letters* 98.21 (2007), p. 216802.

[33] Matthieu C Dartiailh et al. “Missing Shapiro steps in topologically trivial Josephson junction on InAs quantum well”. In: *Nature communications* 12.1 (2021), p. 78.

[34] Liang Jiang et al. “Unconventional Josephson signatures of Majorana bound states”. In: *Physical review letters* 107.23 (2011), p. 236401.

[35] Pauli Virtanen and Patrik Recher. “Microwave spectroscopy of Josephson junctions in topological superconductors”. In: *Physical Review B—Condensed Matter and Materials Physics* 88.14 (2013), p. 144507.

[36] Artem V Galaktionov and Andrei D Zaikin. “Fractional Shapiro steps without fractional Josephson effect”. In: *Physical Review B* 104.5 (2021), p. 054521.

[37] Myung-Ho Bae et al. “Current-phase relationship, thermal and quantum phase slips in superconducting nanowires made on a scaffold created using adhesive tape”. In: *Nano letters* 9.5 (2009), pp. 1889–1896.

[38] SS Ustavschikov and D Yu Vodolazov. “Missing Shapiro steps in nonhysteretic Josephson junction with 2 π periodic supercurrent”. In: *Physical Review B* 110.18 (2024), p. 184511.

[39] Dmitry S Yakovlev et al. “Physical Vapor Deposition Features of Ultrathin Nanocrystals of Bi2 (Te x Se1–x) 3”. In: *The Journal of Physical Chemistry Letters* 13.39 (2022), pp. 9221–9231.

[40] Ivan A Nazhestkin et al. “Enhancing Signal Purity in Josephson Structure Measurements”. In: *Advanced Physics Research* (2025), e2500032.

[41] Hervé Courtois et al. “Origin of hysteresis in a proximity Josephson junction”. In: *Physical review letters* 101.6 (2008), p. 067002.

[42] Torsten Karzig, William S Cole, and Dmitry I Pikulin. “Quasiparticle poisoning of Majorana qubits”. In: *Physical Review Letters* 126.5 (2021), p. 057702.

[43] Peter Russer. “Influence of microwave radiation on current-voltage characteristic of superconducting weak links”. In: *Journal of Applied Physics* 43.4 (1972), pp. 2008–2010.

[44] Konstantin K Likharev. *Dynamics of Josephson junctions and circuits*. Routledge, 2022.

[45] B. Raes et al. “Fractional Shapiro steps in resistively shunted Josephson junctions as a fingerprint of a skewed current-phase relationship”. In: *Phys. Rev. B* 102 (2020), p. 054507.

[46] R Panghotra et al. “Giant fractional Shapiro steps in anisotropic Josephson junction arrays”. In: *Communications Physics* 3.1 (2020), p. 53.

[47] M. Kvale, S. E. Hebboul, and J. C. Garland. “Theory of even-odd step suppression in the RSJ model”. In: *Phys. B Condens. Matter* 165–166 (1990), p. 1585.

[48] Alessandro De Cecco et al. “Interplay between electron overheating and ac Josephson effect”. In: *Physical Review B* 93.18 (2016), p. 180505.

[49] Sophie Charpentier et al. “Induced unconventional superconductivity on the surface states of Bi_2Te_3 topological insulator”. In: *Nature communications* 8.1 (2017), p. 2019.